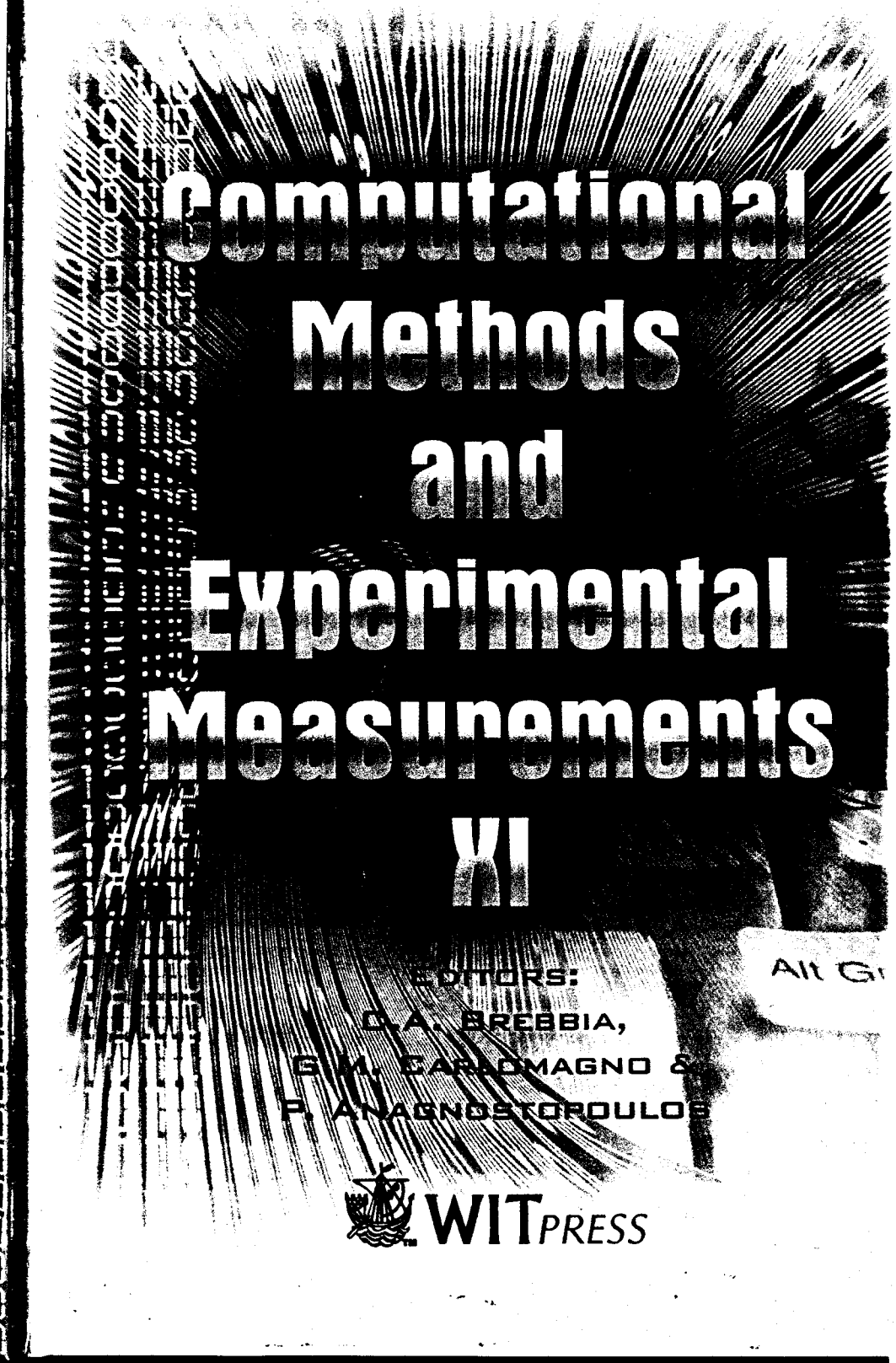
Computational Methods and Experimental Measurements XI
EDITORS:
C.A. BREBBIA,
G.M. CARLOMAGNO &
P. ANAGNOSTOPOULOS
WITPRESS

# Finite length bearings and squeeze-film dampers : A two-dimensional dynamical solution

J. Antunes[1], M. Moreira[2] & P. Piteau[3]
[1] *Institute of Nuclear Technology, Portugal.*
[2] *Politechnic Institute of Setubal, Portugal.*
[3] *Commissariat à l' Energie Atomique, France.*

## Abstract

In this paper we develop a non-linear dynamical solution for finite length bearings and squeeze-film dampers based on a Spectral-Galerkin method.

In this approach the gap-averaged pressure is approximated, in the lubrication Reynolds equation, by a truncated double Fourier series. The Galerkin method, applied over the residuals so obtained, generate a set of simultaneous algebraic equations for the time-dependent coefficients of the double Fourier series for the pressure.

In order to assert the validity of our $2D-$Spectral-Galerkin solution we present some preliminary comparative numerical simulations, which display satisfactory results up to eccentricities of about 0.9 of the reduced fluid gap $H/R$.

The so-called long and short-bearing dynamical solutions of the Reynolds equation, reformulated in Cartesian coordinates, are also presented and compared with the corresponding classic solutions found on literature.

## 1 Introduction

Assuming a viscous flow and neglecting inertial effects, the nonlinear orbital motions — $X(t)$ and $Y(t)$ — of a shaft in a journal bearing, can be described by the Reynolds equation (Frêne et al., [3]; Hamrock, [5]; Antunes, [1])

$$\frac{1}{R^2}\frac{\partial}{\partial\theta}\left(h^3\frac{\partial p}{\partial\theta}\right)+\frac{\partial}{\partial z}\left(h^3\frac{\partial p}{\partial z}\right)=6\mu\left[\Omega\frac{\partial h}{\partial\theta}+2\frac{\partial h}{\partial t}\right] \tag{1}$$

where $h(\theta,z,t)$ is the annulus fluid gap, $\theta$ the azimuth, $z$ the axial coordinate, $t$ time, $\mu$ the dynamic viscosity and $\Omega$ the spinning velocity of the shaft. The main

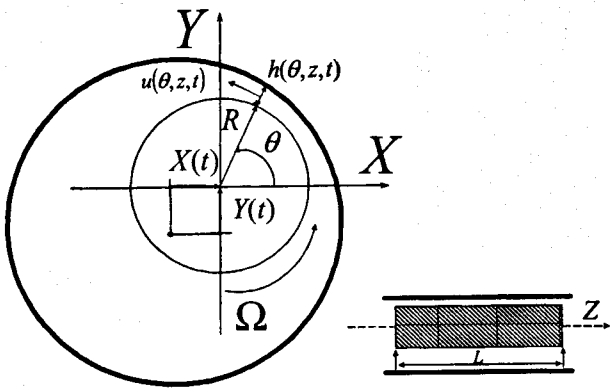


Figure 1: Flow geometry.

geometrical parameters are the shaft radius $R$, the length of the fluid annulus $L$ and the average fluid gap $H$. In Figure 1 we can observe the geometry of the fluid annulus.

Note that a generic two-dimensional analytical solution of (1) is not available. However, classic analytical solutions for two particular limit cases, the long and the short bearing approximations established:

1. the long bearing theory assumes $L/(2R) \gg 1$, yielding

$$\frac{1}{R^2}\frac{\partial}{\partial\theta}\left(h^3\frac{\partial p}{\partial\theta}\right) = 6\mu\left[\Omega\frac{\partial h}{\partial\theta} + 2\frac{\partial h}{\partial t}\right] \tag{2}$$

   by neglecting the axial pressure gradient;

2. the short bearing theory assumes $L/(2R) \ll 1$, yielding

$$\frac{\partial}{\partial z}\left(h^3\frac{\partial p}{\partial z}\right) = 6\mu\left[\Omega\frac{\partial h}{\partial\theta} + 2\frac{\partial h}{\partial t}\right] \tag{3}$$

   by neglecting the azimuthal pressure gradient.

The corresponding analytical solutions (the Sommerfeld solution and the Ocvirk solution) are considered satisfactory approximations when $L/(2R) > 4$ or $L/(2R) < 0.5$, respectively. Unfortunately, most of industrial equipments of interest are characterized by

$$0.5 < L/(2R) < 4.$$

In the following, we will develop a spectral-Galerkin method to obtain two-dimensional pressure solutions for our generic problem (1) – the finite-length journal bearing – from which we shall find the dynamic fluid forces acting on the shaft.



This approach, based on a spatial Fourier series of the pressure $p(\theta,z,t)$ was also considered by Hays [4] and Barret & Allaire [2] for solving the corresponding homogeneous problem:

$$\frac{1}{R^2}\frac{\partial}{\partial\theta}\left(h^3\frac{\partial p}{\partial\theta}\right) + \frac{\partial}{\partial z}\left(h^3\frac{\partial p}{\partial z}\right) = 0. \tag{4}$$

Additionally, for completeness, we will present the a reformulation of the dynamic flow forces acting on the shaft and corresponding to the analytical long-bearing solution of (2) and short-bearing solution of (3).

## 2 Flow formulation

Under the referred assumptions the flow will be modeled using (1).

Consider Figure 1. The annular fluid gap $h(\theta,z,t)$ is very well approximated by

$$h(\theta,z,t) \cong H - X(t)\cos\theta - Y(t)\sin\theta. \tag{5}$$

Note that, approximation (5) assumes the shaft is rigid with a constant circular-cross section and rotation undergoes only translational motions parallel to the journal bearing axis.

We will assume, also, no cavitation and the following boundary conditions

$$p(\theta,0,t) = p(\theta,L,t) = 0. \tag{6}$$

## 3 Galerkin-spectral approach

Consider the spatial Fourier series for the pressure $p(\theta,z,t)$

$$p(\theta,z,t) \sim \sum_{n=1}^{\infty} p_n(\theta,t)\sin\left((2n-1)\pi z/L\right) \tag{7}$$

with

$$p_n(\theta,t) = A_{0n} + \sum_{m=1}^{\infty}\left[A_{mn}(t)\cos(m\theta) + B_{mn}(t)\sin(m\theta)\right] \tag{8}$$

and assume that it converges uniformly to $p$. Clearly, (7) satisfies the postulated boundary conditions also being axially symmetric with respect position $z = L/2$.

Let

$$p(\theta,z,t;N,M) = \sum_{n=1}^{N} p_n(\theta,t;M)\sin\left((2n-1)\pi z/L\right) \tag{9}$$

with

$$p_n(\theta,t;M) = A_{0n} + \sum_{m=1}^{M}\left[A_{mn}(t)\cos(m\theta) + B_{mn}(t)\sin(m\theta)\right] \tag{10}$$

be an approximate solution of (1).

Replacing the truncated series (9) in (1) we obtain a residue

$$R(p(\theta,z,t;N,M)) = \frac{1}{R^2}\frac{\partial}{\partial\theta}\left(h^3(X(t),Y(t),\theta)\frac{\partial p(\theta,z,t;N,M)}{\partial\theta}\right) + \frac{\partial}{\partial z}\left(h^3(X(t),Y(t),\theta)\frac{\partial p(\theta,z,t;N,M)}{\partial z}\right) - 6\mu\Omega\frac{\partial h(X(t),Y(t),\theta)}{\partial\theta} - 12\mu\frac{\partial h(X(t),Y(t),\theta)}{\partial t} \quad (11)$$

which depends on the coefficients $A_{0n}$, $A_{mn}$ and $B_{mn}$ with $m = 1,\ldots,M$ and $n = 1,\ldots,N$. Because (9) is an approximate solution of (1) the residue does not identically vanish. However, (11) will be minimal if it is orthogonal with respect to the vectorial subspace generated by the following $(2M+1)N$ elementary orthogonal functions

$$\{\Psi_{nm} = \sin((2n-1)\pi z/L)\sin(m\theta), n = 1,\ldots,N; m = 1,\ldots,M\} \quad (12)$$
$$\cup\{\Phi_{nm} = \sin((2n-1)\pi z/L)\cos(m\theta), n = 1,\ldots,N; m = 0,1,\ldots,M\}$$

that is, if

$$\langle\Psi_{nm}, R(p[\theta,z,t,N,M])\rangle = 0, n = 1,\ldots,N; m = 1,\ldots,M \quad (13)$$
$$\wedge\langle\Phi_{nm}, R(p[\theta,z,t,N,M])\rangle = 0, n = 1,\ldots,N; m = 0,1,\ldots,M \quad (14)$$

where the inner product is defined as

$$\langle f(\theta,z), g(\theta,z)\rangle = \int_0^{2\pi}\int_0^L f(\theta,z), g(\theta,z)\,dzd\theta. \quad (15)$$

Note that conditions (13) and (14), characterizing the referred Galerkin-spectral approach, generate a system of $(2M+1)N$ algebraic equations. One can show that these equations consist in $N$ non-coupled sets of $2M+1$ coupled algebraic equations (with respect the unknowns $A_{0n}$, $A_{mn}$ and $B_{mn}$ with $m = 1,\ldots,M$ and $n = 1,\ldots,N$), that is, for each $n = 1,\ldots,N$, we obtain the following system

$$\begin{cases} \mathbb{F}_{1,n}\left[A_{0n}, A_{mn}, B_{mn}, m = 1,\ldots,M, n, X, Y, \dot{X}, \dot{Y}\right] = 0 \\ \mathbb{F}_{2,n}\left[A_{0n}, A_{mn}, B_{mn}, m = 1,\ldots,M, n, X, Y, \dot{X}, \dot{Y}\right] = 0 \\ \vdots \\ \mathbb{F}_{2M+1,n}\left[A_{0n}, A_{mn}, B_{mn}, m = 1,\ldots,M, n, X, Y, \dot{X}, \dot{Y}\right] = 0 \end{cases} \quad (16)$$

Interestingly (but understandable as (1) is linear in $p$), system (16) is linear with respect the unknowns $A_{0n}$, $A_{mn}$ and $B_{mn}$ ($m = 1,\ldots,M$ and $n = 1,\ldots,N$), so



we can write it as

$$\mathbf{M}_n(X,Y,n;R,L,H)\begin{Bmatrix} A_{0n} \\ A_{1n} \\ B_{1n} \\ A_{2n} \\ B_{2n} \\ \vdots \\ A_{Mn} \\ B_{Mn} \end{Bmatrix} = \mathbf{C}\left(X,Y,\dot{X},\dot{Y},n;\mathbf{R},L,\mu,\Omega\right) \quad (17)$$

where $\mathbf{M}_n$ is a $(2M+1)\times(2M+1)$ matrix and $\mathbf{C}$ a $(2M+1)$ component column vector. Note that, from (17), we can obtain the coefficients of the Fourier series of the pressure, that is, the approximate non-linear solution of (1), inverting formally $\mathbf{M}_n$ for each $n = 1,\ldots,N$ (in practice, a much more economical numerical solution of (17) can be achieved without inverting $\mathbf{M}_n$):

$$\begin{Bmatrix} A_{0n} \\ A_{1n} \\ B_{1n} \\ A_{2n} \\ B_{2n} \\ \vdots \\ A_{Mn} \\ B_{Mn} \end{Bmatrix} = \mathbf{M}_n^{-1}\mathbf{C}. \quad (18)$$

So, this solution, called here $2D$-Spectral-Galerkin solution for the finite length journal-bearing, will be

$$p(\theta,z,t;N,M) = \sum_{m=0}^{M}\sum_{n=1}^{N}\left[\begin{array}{l} A_{mn}(t)\cos(m\theta)\sin\left((2n-1)\pi\frac{z}{L}\right) \\ +B_{mn}(t)\sin(m\theta)\sin\left((2n-1)\pi\frac{z}{L}\right)\end{array}\right]. \quad (19)$$

## 4 Dynamic flow forces

We are interested in the dynamic flow forces acting on the finite length journal bearing:

$$F_f^X(t) = -\int_0^{2\pi}\int_0^L p(\theta,z,t)\cos(\theta)\,Rd\theta dz, \quad (20)$$
$$F_f^Y(t) = -\int_0^{2\pi}\int_0^L p(\theta,z,t)\sin(\theta)\,Rd\theta dz. \quad (21)$$

These forces can be obtained from expressions (20) and (21), accounting for (19), and one obtains:

$$F_f^X(t;M,N) = -RL\sum_{n=1}^{N}\frac{2}{2n-1}A_{1n}(t), \quad (22)$$

$$F_f^Y(t;M,N) = -RL\sum_{n=1}^{N}\frac{2}{2n-1}B_{1n}(t). \quad (23)$$

Note that the accuracy of (19), (22) and (23) depends on the choice of $N$ and $M$.

Lack of space prevent us from a detailed presentation of the dynamic flow forces for the long-bearing and short-bearing formulations, reformulated in Cartesians coordinates. Their deduction yields (see Moreira et al. [7]):

1. Long-bearing formulation

$$F_f^X(t) = -12\mu LR^3\pi \left\{ \begin{array}{c} \Omega \frac{Y}{(2H^2+X^2+Y^2)\sqrt{H^2-X^2-Y^2}} \\ + \frac{2\dot{X}H^2+\dot{X}X^2-2\dot{X}Y^2+3\dot{Y}XY}{(2H^2+X^2+Y^2)\left(\sqrt{H^2-X^2-Y^2}\right)^3} \end{array} \right\}, \quad (24)$$

$$F_f^Y = 12\mu LR^3\pi \left\{ \begin{array}{c} \Omega \frac{X}{(2H^2+X^2+Y^2)\sqrt{H^2-X^2-Y^2}} \\ - \frac{2\dot{Y}H^2+\dot{Y}Y^2-2\dot{Y}X^2+3\dot{X}XY}{(2H^2+X^2+Y^2)\left(\sqrt{H^2-X^2-Y^2}\right)^3} \end{array} \right\}; \quad (25)$$

2. Short-bearing formulation

$$F_f^X(t) = -\frac{1}{2}\mu RL^3\pi \left\{ \begin{array}{c} \Omega \frac{Y}{\left(\sqrt{H^2-X^2-Y^2}\right)^3} \\ +2\frac{\dot{X}H^2+2\dot{X}X^2-\dot{X}Y^2+3\dot{Y}XY}{\left(\sqrt{H^2-X^2-Y^2}\right)^5} \end{array} \right\}, \quad (26)$$

$$F_f^Y(t) = \frac{1}{2}\mu RL^3\pi \left\{ \begin{array}{c} \Omega \frac{X}{\left(\sqrt{H^2-X^2-Y^2}\right)^3} \\ -2\frac{3\dot{X}XY+\dot{Y}H^2-\dot{Y}X^2+2\dot{Y}Y^2}{\left(\sqrt{H^2-X^2-Y^2}\right)^5} \end{array} \right\}. \quad (27)$$

## 5 Numerical simulations and discussion of results

In order to assert the validity of our $2D$–Spectral-Galerkin solution we present some preliminary comparative numerical simulations. Two different journal-bearing configurations were used in these simulations: a long-bearing configuration with $L/(2R) = 50$ and a short-bearing configuration with $L/(2R) = 1/16$. The main geometrical parameters are given in Table 1.

Table 1: Main geometrical and physical parameters

| Journal-bearing configuration | Long | Short |
|---|---|---|
| $L/(2R)$ | 50 | 1/16 |
| $2R$ (Shaft diameter [m]) | 0.2 | 0.2 |
| $H$ (Annular gap [m]) | $10^{-4}$ | $10^{-4}$ |
| $\mu$ (Dynamic viscosity [Pa.s]) | 0.15 | 0.15 |



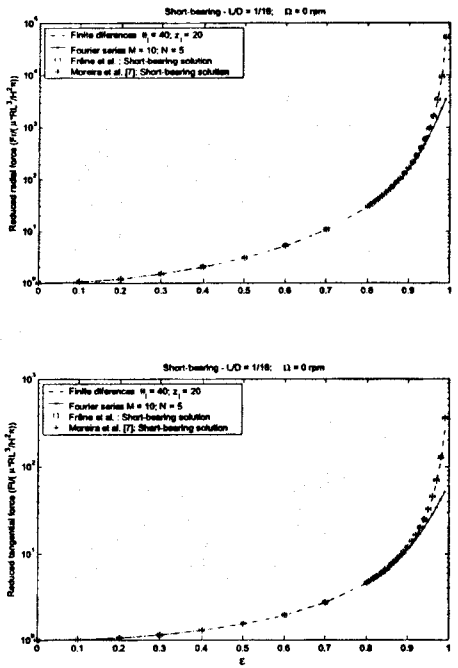


Figure 2: Comparison of finite-difference solutions with the present method using $M = 10$ and $N = 5$ in the $2D$-Spectral-Galerkin model, for a 0 rpm shaft in a short-bearing.

Over each configuration we compare the reduced radial and tangential flow forces, defined as

$$\hat{F}_r = F_r \frac{H^2\pi}{12\mu R^3 L}, \quad (28)$$

$$\hat{F}_t = F_t \frac{H^2\pi}{12\mu R^3 L}. \quad (29)$$

These have been computed using:

1. our $2D$–Spectral-Galerkin solution;
2. a classic finite-diference algorithm with an azimuthal-axial grid of $40 \times 20$;
3. the long and short-bearing solutions presented in Frêne et al. [3];
4. our long and short-bearing solutions reformulations presented in Cartesians coordinate here.

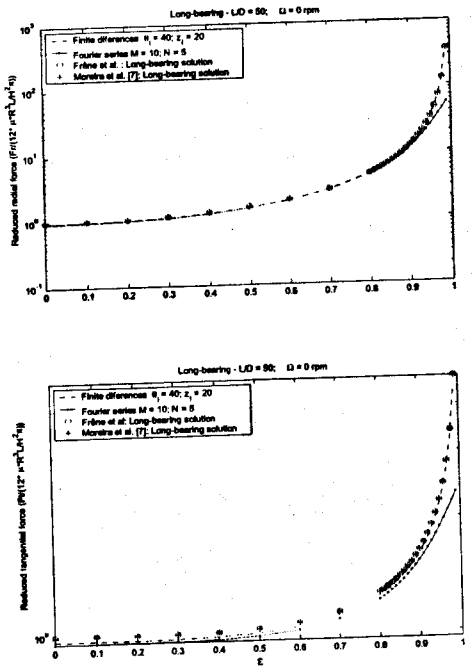


Figure 3: Comparison of finite-difference solutions with the present method using $M = 10$ and $N = 5$ in the $2D$-Spectral-Galerkin model, for a 0 rpm shaft in a long-bearing.

The illustrative computations presented here are based on a eccentered shaft at $X_0 = e$ and $Y_0 = 0$, to which initial velocities $\dot{X}_0 = 0.4$ m/s and $\dot{Y}_0 = 0.4$ m/s were imposed. The instant pressure field and flow forces $F_f^X$ and $F_f^Y$ are computed and displayed in the reduced radial and tangential forms (28) and (29).

In all numerical simulations the predictions are displayed for different reduced eccentricities $0 \leq \varepsilon = \frac{e}{R} \leq 1$. The short and long-bearing approximations are displayed, as well as our $2D-$Spectral-Galerkin model with $M = 10$ azimuthal and $N = 5$ axial terms.

From Figures 3, 2 and 4 we conclude that our $2D-$Spectral-Galerkin model display satisfactory predictions for eccentricities $\varepsilon \leq 0.9$.

For higher eccentricities, our $2D-$Spectral-Galerkin model display increasing errors with eccentricity. However, note that the present computations were performed with a severely truncated series. It is to be expected that higher values of $\varepsilon$ can be properly simulated using more terms.

Note also that, our long and short-bearing solutions reformulated in Cartesian coordinates display the very same predictions of Frêne et al. [3].



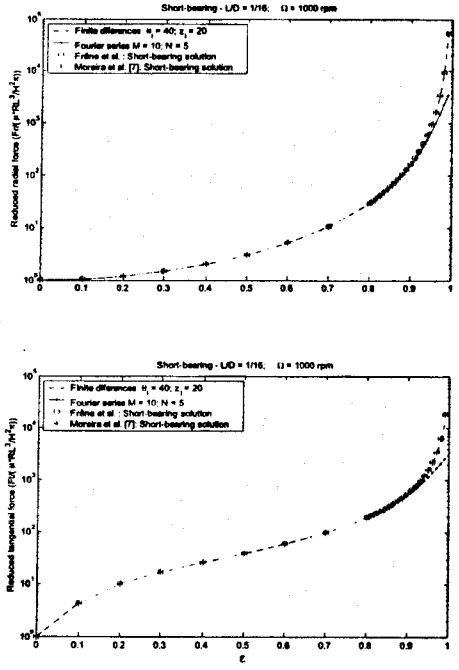


Figure 4: Comparison of finite-difference solutions with the present method using $M = 10$ and $N = 5$ in the $2D$-Spectral-Galerkin model, for a 1000 rpm shaft in a long-bearing.

## 6 Conclusions

In this paper, we developed a non-linear solution of finite length bearings and squeeze-film dampers based on a Galerkin-Spectral approach, called here $2D$ - Spectral - Galerkin solution. By completeness, we reformulated here also, the classic long and short-bearing solutions of the Reynolds equation.

Clearly the accuracy of our solution depend on the number $M$ and $N$ terms used in the truncated Fourier series for the flow pressure. In our preliminary results we found that with a moderate number $M$ and $N$ terms ($M = 10$ and $N = 5$ in short and long-bearing configurations), used in the truncated Fourier series of the flow pressure, we obtained satisfactory predictions, namely up to eccentricities $\varepsilon \leq 0.9$.

For higher eccentricities, $\varepsilon > 0.9$, our $2D$ - Spectral - Galerkin display increasing errors. We anticipate that we needed $M \approx 10 \sim 20$ and $N \approx 5 \sim 10$ terms to obtain satisfactory predictions for this highest range of eccentricities.

Note that the above-mentioned conclusions are also valid when the shaft is spinning (at 1000 rpm in our computations).

Finally, we note that our long and short-bearing reformulated solutions, display the same predictions of the corresponding classic solutions found in Frêne et al. [3].

In future work we will focus on the study of the convergence of this $2D-$Spectral-Galerkin approach. A comparison with the finite differences classic approach is also currently being addressed.

## References

[1] Antunes, J., Dynamics of Rotor-Flow Coupled Systems, in Flow Induced Vibration (P. Anagnastopoulos, Ed.), WIT Press, Southamton.

[2] Barret, D. L. & Allaire, P., Analytical Nonlinear Bearing Calculations using a Variational Approach, Vibration in rotating machinery, Institute of Mechanical Engineers, C287/80, pp. 247-252.

[3] Frêne, J., Nicolas, D., Deguerce, B., Berthe & Godet, M., Lubrification Hydrodynamique: Paliers et Butées, Editions Eyrolles, Pareis, 1990.

[4] Hays, D., A Variational Approach to Lubrication Problems and the Solution of the Finite Journal Bearings, ASME Journal of basic Engineering, Vol. 81, pp. 13-23.

[5] Hamrock, B., Fundamentals of Fluid Film Lubrication, Mc-Graw Hill, New-York, 1994.

[6] Moreira, M., Antunes, J. & Pina H. A Theoretical model for nonlinear orbital motions of rotors under fluid confinement. *Journal of Fluid and Structures* **14**, pp. 635-668, 2000.

[7] Moreira, M., Antunes, J. & Piteau, P., A Theoretical Series Solution for the Dynamics of Finite-Length Bearings and Squeeze-film dampers, to appear in 2003.

[8] Ocvirk, F. & Dubois, G., Analytical Derivation and Experimental Evaluation of Short Bearing Approximations of Full Journal Bearings, NACA Technical Report 1157.

[9] Sommerfeld, A., Zur Hydrodynamischen Theorie der Schiermittelreibung, Z. A. Math. Phys., Vol. 50, pp. 97-155.

# An experimental study on the flow within two disks

P. Tsifourdaris, G.H. Vatistas & W. Ghaly
*Mechanical and Industrial Engineering Department, Concordia University, Canada*

## Abstract

The present experimental study concerns the flows generated within the gap of two parallel disks. For the sink-flow the reduction of the cross-sectional area along the flow direction drives the average velocity to increase which is accompanied by a static pressure drop. Due to the non-slip requirement on the upper and lower disks, a boundary layer forms. Increase of the local inertia to viscous forces ratio forces the radial velocity profile to flatten mid-channel. As the radius becomes smaller, the plateau progressively expands towards the wall. The source-flow in comparison to sink-flow, exhibits a reverse behavior of the pressure along the flow direction. However, there is a special phenomenon associated with this type of flow field, which is absent in the previous case. Fluid particles near the walls, moving within an adverse pressure gradient, experience a flow reversal. The later produces a vortex that is clearly evident in the pressure profile. The experimental pressure profiles for sink- and source-flows with swirl indicate a pressure variation qualitatively similar to that without swirl, but the generated strong vortex makes the drop more dramatic. Reasonable correlation for the inflow with the previously developed theory is apparent.

## 1 Introduction

A range of fundamentally different in flows can evolve within the gap formed by the two disks shown in Fig. 1. Letting the fluid enter the gap from the periphery, and to exit through centrally located outlet(s) generates the accelerating (or sink) flow. This type undergoes a monotonically decreasing pressure gradient, whereby the favorable effects of acceleration encourages the